UNLV | UNIVERSITY LIBRARIES

Mechanical Engineering Faculty Publications | Mechanical Engineering

2010

On the Effect of Hydrodynamic Slip on the Polarization of a Nonconducting Spherical Particle in an Alternating Electric Field

Hui Zhao
University of Nevada, Las Vegas, hui.zhao@unlv.edu

Follow this and additional works at: https://digitalscholarship.unlv.edu/me_fac_articles

Part of the Electrical and Computer Engineering Commons, Mechanical Engineering Commons, and the Nanoscience and Nanotechnology Commons

Repository Citation

Zhao, H. (2010). On the Effect of Hydrodynamic Slip on the Polarization of a Nonconducting Spherical Particle in an Alternating Electric Field. *Physics of Fluids, 22*(7), 1-15.
https://digitalscholarship.unlv.edu/me_fac_articles/557

This Article is protected by copyright and/or related rights. It has been brought to you by Digital Scholarship@UNLV with permission from the rights-holder(s). You are free to use this Article in any way that is permitted by the copyright and related rights legislation that applies to your use. For other uses you need to obtain permission from the rights-holder(s) directly, unless additional rights are indicated by a Creative Commons license in the record and/or on the work itself.

This Article has been accepted for inclusion in Mechanical Engineering Faculty Publications by an authorized administrator of Digital Scholarship@UNLV. For more information, please contact digitalscholarship@unlv.edu.

AIP | Physics of Fluids

On the effect of hydrodynamic slip on the polarization of a nonconducting spherical particle in an alternating electric field

Hui Zhao

Citation: Phys. Fluids **22**, 072004 (2010); doi: 10.1063/1.3464159
View online: http://dx.doi.org/10.1063/1.3464159
View Table of Contents: http://pof.aip.org/resource/1/PHFLE6/v22/i7
Published by the AIP Publishing LLC.

Additional information on Phys. Fluids

Journal Homepage: http://pof.aip.org/
Journal Information: http://pof.aip.org/about/about_the_journal
Top downloads: http://pof.aip.org/features/most_downloaded
Information for Authors: http://pof.aip.org/authors

ADVERTISEMENT

Downloaded 13 Aug 2013 to 131.216.164.149. This article is copyrighted as indicated in the abstract. Reuse of AIP content is subject to the terms at: http://pof.aip.org/about/rights_and_permissions

On the effect of hydrodynamic slip on the polarization of a nonconducting spherical particle in an alternating electric field

Hui Zhao[a)]
Department of Mechanical Engineering, University of Nevada, Las Vegas, Nevada 89154, USA

(Received 8 December 2009; accepted 23 June 2010; published online 28 July 2010)

The polarization of a charged, dielectric, spherical particle with a hydrodynamically slipping surface under the influence of a uniform alternating electric field is studied by solving the standard model (the Poisson–Nernst–Planck equations). The dipole moment characterizing the strength of the polarization is computed as a function of the double layer thickness, the electric field frequency, the particle's surface charge, and the slip length. Our studies reveal that two processes contribute to the dipole moment: ion transport inside the double layer driven by the electric field and the particle's electrophoretic motion. The hydrodynamic slip will simultaneously impact both processes. In the case of a thick double layer, an approximate analytical expression for the dipole moment of a weakly charged particle with an arbitrary slip length and a small zeta potential ζ [normalized with the thermal voltage ($\sim$25 mV)], accurate within $O(\zeta^2)$, shows that the polarization is dominated by the particle's electrophoretic motion and the enhancement of the polarization due to the hydrodynamic slip is primarily attributed to the enhancement of the electrophoretic mobility from the slip. In contrast, for a thin double layer, the dipole moment is governed by ion transport inside the double layer. Asymptotical analytical models conclude that the hydrodynamic slip has more complicated influence on the polarization. At the high-frequency range where the surface conduction is important, the dipole moment is predicted to increase for any zeta potential. On the contrary, at the low-frequency range where the bulk diffusion is significant, the enhancement of the dipole moment due to the slip is lost at large zeta potentials. © *2010 American Institute of Physics*.
[doi:10.1063/1.3464159]

I. INTRODUCTION

Recently, there has been a growing interest in using alternating-current (ac) electric fields to manipulate, separate, and assemble nanoparticles[1–4] and biomolecules[5,6] and to drive and stir fluids in lab-on-a-chip systems.[7–11] For instance, ac electric fields can be used to align and pattern CdSe nanoparticles on silicon substrates to form colloidal crystals of desired electric and optical properties, which has potential applications in designing high-efficiency photovoltaic solar cells.[12,13] Nanoparticle assembly can also serve as disposable, low-cost, miniaturized biosensors.[14] To further exploit the advantages of the electric field, the properties of manipulated particles, in particular, surface properties when particles are suspended in an electrolyte solution, need to be understood.

The solid-liquid surface has many intriguing hydrodynamic features. The conventional nonslip boundary condition is based on empirical knowledge. With the advance of the nanofabrication technology and novel, sensitive, high-resolution experimental techniques, slip over hydrophobic surfaces has been detected in experiments and slip length was measured around the order of nanometers.[15–21] Experiments and molecular simulations also revealed that an electro-osmotic flow over a charged slipping surface can be significantly boasted by the slip compared to their nonslip counterpart.[22–25] The electro-osmotic flow over a slipping surface has many applications ranging from drag reduction,[26,27] nanoscale energy conversion,[28,29] to electrochromatography.[30] Thus, studying electrokinetic flows over a slipping surface attracts many attentions.[31,32]

The effect of the slip has been studied over inhomogeneously charged slipping surfaces[33] and the diffusio-osmotic flow induced by a solute concentration gradient over a superhydrophobic surface was predicted to be massively amplified.[34,35] Studies of the influence of the hydrodynamic slip on particle's motion also has begun. Different phoretic motions of charged particles have been investigated including diffuisophoresis, thermophoresis, as well as electrophoresis.[35–37] Previous studies found out that in the limit of thin double layers, the hydrodynamic slip enhances the electrophoretic mobility only for small and moderate zeta potentials, and such enhancement of hydrodynamic slip is lost at high zeta potentials due to nonuniform surface conduction and concentration polarization outside the double layer.[37]

Dielectrophoresis is the most popular and promising technique to manipulate nanoparticles and biomolecules in an ac field due to its inherent advantages (i.e., the precise ability to control magnitude of the forces on nanoparticles, suitable integration into lab-on-a-chip systems, and low fabrication cost[38]). This technique was also suggested to probe surface properties of nanoparticles and biomolecules.[6] Therefore, it is worthwhile to investigate the influence of the

[a)]Author to whom correspondence should be addressed. Electronic mail: hui.zhao@unlv.edu.

 © 2010 American Institute of Physics

Downloaded 13 Aug 2013 to 131.216.164.149. This article is copyrighted as indicated in the abstract. Reuse of AIP content is subject to the terms at: http://pof.aip.org/about/rights_and_permissions

hydrodynamic slip on dielectrophoretic motion of charged particles.

Since the dielectrophoretic motion inherently relies on the particle's polarization, the objective of this article is to examine the influence of the hydrodynamic slip on the polarization of a charged dielectric particle whose surface exhibits apparent slip under the action of an ac electric field for an arbitrary double layer thickness, slip length, as well as zeta potential over a broad range of frequencies. Recent experiments revealed that the dielectrophoretic tension inside actin filaments induced by the polarization under the action of an ac field is orders of magnitude larger than that predicted by the theory, assuming that the surface of actin filaments is nonslip.[6] Considering that a considerable portion of the surface of actin filaments contains hydrophobic patches,[39] the hydrodynamic slip might be able to bridge the discrepancy between experimental results and theoretical predictions if the polarization can be enhanced by the slip under certain conditions as it does to the electrophoretic mobility.

First let us review several fundamental aspects of dielectrophoresis in the absence of the slip. Under the action of an electric field when a particle is submerged into either a dielectric or conducting medium (i.e., an electrolyte solution), it polarizes and develops a dipole moment. In the presence of a nonuniform electric field, the poles of the dipole are subjected to different electric field intensities, a net force is induced, and leads to a particle's motion termed dielectrophoresis (DEP).[40–42] In contrast to an electrophoretic motion which disappears in an ac field, the dielectrophoretic motion, whose velocity is proportional to the square of the electric field, prevails in an ac field. In a nonuniform electric field, when a particle is more polarizable than the medium corresponding to a positive dipole moment, the particle will be attracted to the location of the electric field maximum. The particle with a negative dipole moment less polarizable than the medium will be repelled from the location of the electric field maximum.

When suspended in an electrolyte solution, a charged particle is typically enveloped with an electric double layer.[43,44] In the presence of an electric field, excess counterions inside the double layer migrate, drag water molecules with them, and result in an electro-osmotic flow, which, in turn, transports ions. Ions' migration and convection consist of an ionic current along the particle's surface which polarizes the double layer and modifies the dipole moment [Fig. 1(a)]. At the same time, the electrophoretic motion of the particle in response to the applied electric field attempts to squeeze the double layer near one end of the particle and relax the double layer at the other end [Fig. 1(b)].[45–47] This squeezing-relaxing process also polarizes the double layer and changes the strength of the dipole moment.

To predict the dipole moment determined by the double layer polarization of a charged dielectric particle, researchers often use the Maxwell–Wagner–O'Konski (MWO) theory.[48] Briefly, the theory accounts for the polarization due to the difference between the electric properties of the particle and the suspending medium and due to ions' migration and convection in the double layer which is approximated as a surface conductivity. For instance, when the size of the particle is small compared to the characteristic length of the electric field's variations, the MWO model estimates the force acting on the particle: $\vec{F}^* = 3/2 V^* \varepsilon_1^* \,\mathrm{Re}(f) \nabla \vec{E}^{*2}_{\mathrm{RMS}}$,[48] where V^* is the particle's volume; $\vec{E}^*_{\mathrm{RMS}}$ is the electric field's intensity at the location of the particle's center (in the particle's absence); $f = (\bar{\varepsilon}_2^* - \bar{\varepsilon}_1^*)/(2\bar{\varepsilon}_1^* + \bar{\varepsilon}_2^*)$ is the Clausius–Mossoti factor for a spherical particle; $\bar{\varepsilon}_i^* = \varepsilon_i^* - i(\kappa_i^*/\omega^*)$ is the complex permittivity; ε_i^* is the dielectric permittivity; κ_i^* is the conductivity which includes the surface conduction induced by ions' migration and convection inside the double layer; ω^* is the electric field's frequency; $\mathrm{Re}(f)$ denotes the real part of f; and subscripts $i=1$ and 2 refer, respectively, to the suspending medium and the particle.

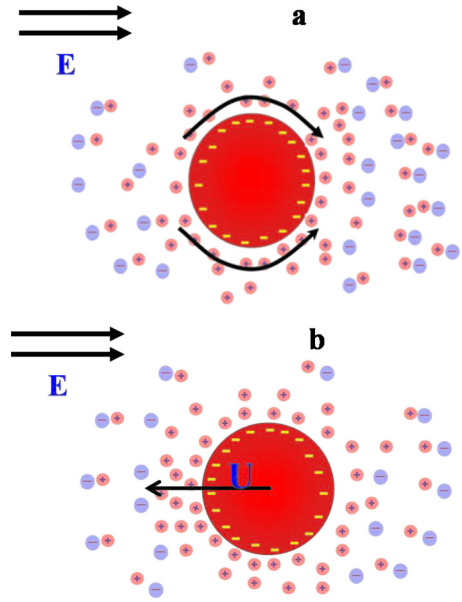

FIG. 1. (Color online) A schematic of the polarization of the double layer surrounding a negatively charged, dielectric particle. (a) The double layer polarization is caused by ion migration and convection under the influence of the applied electric field; (b) the polarization is attributed to the particle's electrophoretic motion. The arrows indicate the direction of counterion motion.

However, the MWO model does not consider the diffusion of ions outside the double layer and, therefore, is valid only at high frequencies and thin electric double layers.[46,49–51] To account for the influence of the bulk diffusion on the dipole moment, the Ukraine school[52,53] developed a theory for low-frequency dispersion [the Dukhin–Shilov (DS) theory] under the assumption that the double layer is at local equilibrium with the surrounding bulk solution. The DS theory is thus only applicable at low frequencies where ions have enough time to reach local equilibrium.

Both the MWO and DS theories are restricted to electric double layers that are thin compared to the particle's radius.[51] In addition, both the MWO and DS theories assume that the particle is immobile. In other words, both theories do not consider the influence of the electrophoretic motion on the dipole moment. It was numerically verified that when $\lambda_D \leq 0.1$ (normalized with the particle's radius),[45] the assumption of the immobile particle holds and in the case of

Downloaded 13 Aug 2013 to 131.216.164.149. This article is copyrighted as indicated in the abstract. Reuse of AIP content is subject to the terms at: http://pof.aip.org/about/rights_and_permissions

$\lambda_D > 0.1$, the contribution of the particle's electrophoretic motion to the dipole moment is appreciable. In particular, in the limit of thick double layers ($\lambda_D \gg 1$), Zhao and Bau[47] derived an approximate expression for the dipole moment of a weakly charged, dielectric particle, suggesting that the contribution of the electrophoretic motion is dominant and the dipole moment exhibits a qualitative distinction from that of the thin double layer.

For a moderate double layer thickness, to correctly predict the particle's polarization, it is required to numerically solve the Poisson–Nernst–Planck (PNP) equations. The PNP model has been used extensively to calculate the dipole moment of spherical particles,[46,47,54–65] long (two-dimensional) cylindrical particles with the electric field transverse to their axis,[51] and elongated cylindrical particles with the electric field along their axis.[66] The predictions from the PNP model have an excellent agreement with the MWO and DS models over different frequency ranges in the limit of thin double layers. Moreover, the PNP model agreed well with experiments in the case of thick double layers.[47,67] In summary, the PNP model is adequate to calculate the dipole moment of a nonslip particle accounting for ions' migration, convection, diffusion, as well as particle's electrophoretic motion. Thus it is also appropriate to use the PNP model to investigate the role of the hydrodynamic slip in particle's polarization.

Bazant and co-workers[68–70] studied the polarization of uncharged, metallic particles under the action of an electric field, which was also extensively documented in Russian literature.[71–74] In this case, the applied electric field polarizes the conducting particle and induces surface charges which attract counterions, forming an induced double layer. The interaction between the double layer and the external electric field generates a body force, which induces an electroosmotic flow when the particle is fixed, and causes particle to migrate when the particle is free to move.[70,75] In contrast, in this paper, the electric double layer (EDL) is formed due to free surface charges and is not induced. Since the dielectric constant of the particle is quite small, the induced charge effect is negligible.

This article is organized as follows. Section II introduces the PNP (standard) model accounting for ions' migration, convection, diffusion, as well as the hydrodynamic slip on the particle's surface. Section III presents a regular perturbation expansion in terms of the applied electric field's magnitude (i.e., the applied electric field is assumed to be small compared to the electric field associated with the free surface charge inside the double layer) and derives the dipole moment from the first order electric potential. In Sec. IV, we further expand variables in terms of the ζ potential to derive an approximate expression for the dipole moment coefficient for small zeta potentials and thick double layers. The detailed derivation is presented in Appendix A. Section V extends the standard MWO and DS models to incorporate the influence of the slip in the case of thin double layers. The detailed derivation of the DS model is delegated to Appendix B. In Sec. VI, the perturbed, first order PNP equations are solved numerically and so is the dipole moment for an arbitrary double layer thickness, slip length, as well as zeta potential.

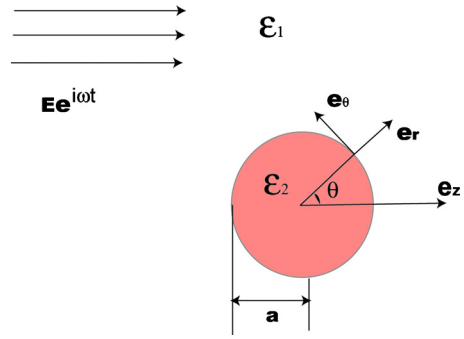

FIG. 2. (Color online) A schematic of the geometry and the coordinate system.

Numerical predictions from the PNP model are favorably compared with those obtained in Secs. IV and V, therefore, in turn, validating our approximate expressions. Section VII concludes.

II. MATHEMATICAL MODEL

Consider a uniformly charged dielectric spherical particle with radius a^* and permittivity ε_2^* freely suspended in a symmetric electrolyte with permittivity ε_1^*. A uniform ac electric field $-\varphi_\infty^* e^{i\omega^* t}\hat{e}_z$ is imposed far from the particle. The superscript * denotes the dimensional form of the various variables. Variables without the superscript * are dimensionless. The electric field electrophoresizes the charged particle to oscillate around its center with a velocity $\vec{U}^*(t) = U_0^* e^{i\omega^* t}$ parallel to the z-coordinate. To facilitate the computation, we use the Galilean transformation $z^* \to z^* - \int^t \vec{U}^*(\xi) d\xi$ to fix the origin of the coordinate system at the particle's center. The particle's velocity $\vec{U}^*$ is not known *a priori* and needs to be determined as part of the solution process. We use the spherical (r, θ, ϕ) coordinate system with its origin fixed at the center of the particle. In the above, θ is the angle between e_r and e_z. Figure 2 depicts the geometry and the coordinate system.

The applied electric field imposes a Coulomb force on ions in the solution. Excess counterions inside the EDL migrate, drag the water with them, and induce an electroosmotic flow. Simultaneously, the charged particle is driven by the electric field to experience an electrophoretic motion which also drags the surrounding liquid to move. Since the typical Reynolds number associated with electrokinetic flows is small, the flow velocities satisfy the Stokes equation

$$\mathrm{Sc}\left(\frac{\partial \vec{u}}{\partial t} + \frac{dU_0 e^{i\omega t}}{dt}\right) = -\nabla p - \frac{1}{2\lambda_D^2}(C_+ - C_-)\nabla \varphi_1 + \nabla^2 \vec{u}. \tag{1}$$

The fluid is incompressible

$$\nabla \cdot \vec{u} = 0. \tag{2}$$

In the above, all the variables are dimensionless. The various scales used in the normalization scheme will be specified later. t is time; p is the pressure; C is the ion's concentration; the subscripts $(+)$ and $(-)$ denote, respectively, the cations

Downloaded 13 Aug 2013 to 131.216.164.149. This article is copyrighted as indicated in the abstract. Reuse of AIP content is subject to the terms at: http://pof.aip.org/about/rights_and_permissions

and the anions; φ is the electric potential; $\vec{E}=-\nabla\varphi$ is the electric field; subscripts 1 and 2 denote, respectively, the liquid and the particle; $\lambda_D=1/a^*\sqrt{(\varepsilon_1^* R^* T^*)/(2F^{*2}C_0^*)}$ is the dimensionless Debye screening length normalized with the particle's radius a^*; C_0^* is the solute's bulk concentration; R^* is the ideal gas constant; F^* is the Faraday constant; T^* is the temperature; $\mathrm{Sc}=D_+^*/\nu^*$ is the Schmidt number; D_+^* is the cation's diffusivity; and ν^* is the solvent's kinematic viscosity. We are more interested in a frequency range such that $Sc\omega$ is so small that the inertia term in Eq. (1) can be neglected.

The electric potential φ in the liquid obeys the Poisson equation

$$\nabla^2\varphi_1=-\frac{C_+-C_-}{2\lambda_D^2}. \tag{3}$$

The particle's electric potential satisfies the Laplace equation

$$\nabla^2\varphi_2=0. \tag{4}$$

The ions' fluxes

$$\vec{N}_\pm=-D_\pm\nabla C_\pm-z_\pm D_\pm C_\pm\nabla\varphi_1+PeC_\pm\vec{u} \tag{5}$$

satisfy the Nernst–Planck equations

$$\frac{\partial C_\pm}{\partial t}+\nabla\cdot\vec{N}_\pm=0. \tag{6}$$

In the above, $Pe=(\varepsilon_1^* R^{*2}T^{*2})/(\mu^* D_+^* F^{*2})$ is the Peclet number and μ^* is the solvent's dynamic viscosity.

At the far field,

$$\varphi_1=-\delta\varphi_\infty r\cos\theta e^{i\omega t},\quad C_\pm=1,\quad \text{and}$$
$$\vec{u}=-U_0e^{i\omega t}e_z\quad (r\to\infty). \tag{7}$$

Due to the free charge (σ) on the particle's surface, there is a jump in the dielectric displacement.

$$\frac{\partial\varphi_1}{\partial n}-\varepsilon_r\frac{\partial\varphi_2}{\partial n}=\sigma,\quad \varphi_1-\varphi_2=0,\quad \text{and}$$
$$\vec{n}\cdot\vec{N}_\pm=0\quad (r=1). \tag{8}$$

In the above, $\varepsilon_r=\varepsilon_2^*/\varepsilon_1^*$ is the relative permittivity, $\vec{n}$ denotes the outer normal vector to the surface, and $\varepsilon_r\ll 1$. We assume that the particle is nonconducting, preclude any Faradic reactions on the particle's surface, neglect conduction in the Stern layer, and assume that the free surface charge is independent of the applied electric field.

Because the particle's surface is assumed to be slipping, the slip at solid-liquid interface can be modeled by the Navier boundary condition where the slip velocity $\vec{u}_\tau$ is proportional to the local shear stress

$$\vec{u}_\tau=\beta\vec{n}\cdot(\nabla\vec{u}+(\nabla\vec{u})^T)\cdot(I-\vec{n}\vec{n}), \tag{9}$$

where β is the dimensionless slip length normalized with the particle's radius.

We also require the potential at the particle's center ($r=0$) to be finite. The particle's electrophoretic velocity U_0 will be determined by nullifying the forces acting on the particle.

In the above, we use the particle's radius a^* as the length scale; R^*T^*/F^* as the electric potential scale; $\varepsilon_1^* R^{*2}T^{*2}/(\mu^* F^{*2}a^*)$ as the velocity scale; the bulk concentration C_0^* as the concentration scale; a^{*2}/D_+^* as the time scale; $\varepsilon_1^* R^{*2}T^{*2}/(F^{*2}a^{*2})$ as the pressure scale; $\varepsilon_1^* R^*T^*/(F^*a^*)$ as the electric charge scale; and $D_+^* C_0^*/a^*$ as the mass flux scale. $D_\pm=D_\pm^*/D_+^*$ is the ratio of the molecular diffusivities (i.e., $D_+=1$). Below, for simplicity, we will assume $D_+=D_-$ (it is straightforward to extend to the case of $D_+\neq D_-$).

III. PERTURBATION EXPANSION IN TERMS OF THE APPLIED ELECTRIC FIELD'S INTENSITY

We consider a nonconducting, spherical particle subjected to a weak, external electric field. The external electric field disturbs only slightly the electric potential and the ion concentrations of the equilibrium electric double layer. In other words, the imposed electric field is much smaller than the electric field inside the equilibrium electric double layer. Thus, we can use a regular perturbation expansion in terms of the applied electric field about the equilibrium double layer

$$\begin{pmatrix}\varphi\\ C_\pm\\ \vec{u}\end{pmatrix}=\begin{pmatrix}\varphi_1^{(0)}\\ C_\pm^{(0)}\\ 0\end{pmatrix}+\delta\,\mathrm{Re}\left[\begin{pmatrix}\varphi_1^{(1)}\\ C_\pm^{(1)}\\ \vec{u}^{(1)}\end{pmatrix}e^{i\omega t}\right]+\mathrm{O}(\delta^2). \tag{10}$$

In the above, δ is the ratio between the magnitude of the external electric field and that associated with the equilibrium electric double layer ($\varphi^\infty\lambda_D/\zeta$). For example, for a charged particle with a zeta potential 50 mV suspended in a 10 mM KCl solution, the electric field generated by the equilibrium EDL is about 10^7 V/m in comparison with 10^4 V/m usually generated by the applied electric field in a microfluidic device. The symbol Re indicates the real part of a complex variable, and $i=\sqrt{-1}$. To calculate the particle's unknown electrophoretic velocity $\vec{U}$, we will balance the forces acting on the particle.

A. The zeroth order approximation

We assume that $\varphi^{(0)}$ and $C_\pm^{(0)}$ be, respectively, the equilibrium electric potential and the equilibrium concentrations induced by the free surface charge in the absence of an external electric field. At equilibrium, the fluid is at rest. Thus the zeroth order velocities are zero.

Since the zeroth order problem is axisymmetric, the zeroth order variables depend only on the radial coordinate (r). At equilibrium, the ions' concentrations $C_\pm^{(0)}$ obey the Boltzmann distribution

$$C_\pm^{(0)}=e^{\mp\varphi_1^{(0)}}. \tag{11}$$

The electric potential $\varphi_1^{(0)}$ satisfies the Poisson–Boltzmann equation

Downloaded 13 Aug 2013 to 131.216.164.149. This article is copyrighted as indicated in the abstract. Reuse of AIP content is subject to the terms at: http://pof.aip.org/about/rights_and_permissions

$$\frac{1}{r^2}\frac{d}{dr}\left(r^2\frac{d\varphi_1^{(0)}}{dr}\right)=\frac{\sinh(\varphi_1^{(0)})}{\lambda_D^2}. \tag{12}$$

The corresponding boundary conditions are

$$\varphi_1^{(0)}(1)-\zeta=\varphi_1^{(0)}(\infty)=0. \tag{13}$$

B. The first order approximation

The weak, applied, external electric field slightly perturbs the equilibrium electric double layer. The first order equations are linear in the perturbed quantities and therefore the dependent variables oscillate at the forcing frequency. Further, accounting for the linearity of the first order governing equations, we can decompose the $O(\delta)$ problem into two subproblems: (1) the **E** problem consisting of a sphere held stationary in the presence of the same electric field as the original problem at infinity and (2) the **U** problem consisting of a sphere at rest in a uniform flow field in the absence of the external electric field.[76] Accordingly, the solutions of the first order problem can be written as the superposition

$$X^{(1)}=(X^{(1)E}+U_0X^{(1)U})e^{i\omega t}. \tag{14}$$

In the above, X stands for any of the dependent variables and the superscripts **E** and **U** denote, respectively, the solutions of the **E** and **U** problems. Considering that most equations (but not all the boundary conditions) are identical for the **E** and **U** problems, we drop the superscripts **E** and **U**, and will use the superscripts **E** and **U** only when it is necessary to distinguish the boundary conditions which are only applicable to one of the problems but not the other.

Substituting series (10) into Eqs. (1)–(6), retaining terms up to $O(\delta)$, and replacing the time derivative with $i\omega$, we obtain

$$-\nabla p^{(1)}-\frac{1}{2\lambda_D^2}[(C_+^{(0)}-C_-^{(0)})\nabla\varphi_1^{(1)}+(C_+^{(1)}-C_-^{(1)})\nabla\varphi_1^{(0)}]+\nabla^2\vec{u}^{(1)}=0, \tag{15}$$

$$\nabla\cdot\vec{u}^{(1)}=0, \tag{16}$$

$$\nabla^2\varphi_1^{(1)}=-\frac{C_+^{(1)}-C_-^{(1)}}{2\lambda_D^2}, \tag{17}$$

$$\nabla^2\varphi_2^{(1)}=0, \tag{18}$$

and

$$i\omega C_\pm^{(1)}+\nabla\cdot(-\nabla C_\pm^{(1)}-z_\pm(C_\pm^{(0)}\nabla\varphi_1^{(1)}+C_\pm^{(1)}\nabla\varphi_1^{(0)})+PeC_\pm^{(0)}\vec{u}^{(1)})=0. \tag{19}$$

The boundary conditions on the particle's surface $(r=1)$

$$\varepsilon_r\frac{d\varphi_2^{(1)}}{dr}-\frac{d\varphi_1^{(1)}}{dr}=-\frac{dC_\pm^{(1)}}{dr}-z_\pm\left(C_\pm^{(0)}\frac{d\varphi_1^{(1)}}{dr}+C_\pm^{(1)}\frac{d\varphi_1^{(0)}}{dr}\right)=0 \tag{20}$$

and

$$u_\theta^{(1)}=\frac{\beta}{1+\beta}\frac{du_\theta^{(1)}}{dr},\quad u_r^{(1)}=0, \tag{21}$$

are identical for both the **E** and **U** problems. The far field boundary conditions are, respectively,

$$\varphi_1^{(1)E}+\varphi_\infty r=\vec{u}^{(1)E}=C_\pm^{(1)E}=0\quad\text{at}\ r\to\infty \tag{22}$$

and

$$\hat{\varphi}_1^{(1)U}=\vec{u}^{(1)U}-e_z=C_\pm^{(1)U}=0\quad\text{at}\ r\to\infty \tag{23}$$

for the **E** and **U** problems.

Consider the form of the electric field, Eqs. (15)–(23) can be further simplified to ordinary differential equations.[47] We solved the ordinary differential equations with the commercial finite element software COMSOL 3.5 (Comsol™, Sweden). The computational domain consisted of a finite domain $0\le r\le R$. We selected $R=10^4$ since further increase in R resulted in little variations, which suggests that R is sufficiently large to render the computational results reasonably R-independent. In order to resolve the detailed structure of the electric double layer, nonuniform elements were used with a dense mesh concentrated next to the particle's surface and the elements' size gradually increasing as the distance from the particle increases. The mesh was refined a few times to assure that the computational results are mesh-independent.

C. The dipole moment coefficient

The particle and its adjacent electric double layer perturb the electric field. Far from the particle, the perturbed field appears like a field induced by a dipole and the electric potential admits the form $\delta\phi_\infty(-r+f/r^2)\cos\theta$, where the real part of f is the dipole coefficient. The dipole coefficient $\mathrm{Re}(f)$ is a function of the zeta potential, the double layer thickness, the slip length, and the electric field's frequency. $\mathrm{Re}(f)$ can be calculated from the behavior of the potential $\varphi_1^{(1)}$ as a function of r sufficiently far from the particle, which remains constant over $1\ll r\ll R$.

To verify the computational algorithm, we calculated the dipole moment f for various values of λ_D and ζ in the absence of the slip and obtained excellent agreements with computational results reported in literature.[46,47] Moreover, our computed dipole moments agreed well with the ones predicted by analytical models for both thick double layers and thin double layers (Figs. 3 and 6).

IV. THE DIPOLE MOMENT FOR THICK DOUBLE LAYERS AND SMALL ZETA POTENTIALS

When the ζ potential of the charged particle is small, the first order, dependent variables can be further expanded into a series in terms of ζ and the corresponding equations can be solved analytically.[47,55,77–79]

In the case of a weakly charged particle $|\zeta|\ll 1$ with a small dielectric constant, O'Brien[55] derived an implicit expression for the dipole moment coefficient applicable for arbitrary double layer thicknesses. However, O'Brien's method requires one to solve an ordinary differential equation numerically. In the limit of thick double layers $(\lambda_D\gg 1)$, Zhao

Downloaded 13 Aug 2013 to 131.216.164.149. This article is copyrighted as indicated in the abstract. Reuse of AIP content is subject to the terms at: http://pof.aip.org/about/rights_and_permissions

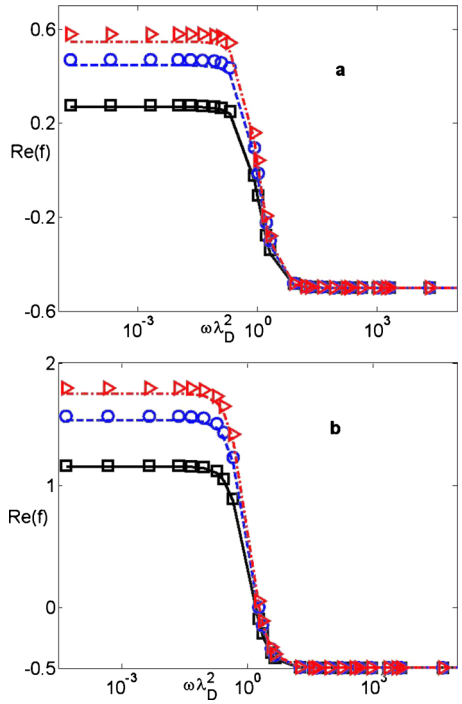

FIG. 3. (Color online) The dipole coefficient as a function of $\omega\lambda_D^2$: (a) $\lambda_D=10$ and (b) $\lambda_D=15$, where $\zeta=-0.2$. The solid line, the dashed line, and the dashed-dotted line correspond, respectively, to $\beta=0.1$, $\beta=1$, and $\beta=10$. The lines and symbols are, respectively, predictions based on Eq. (24) and the PNP model.

and Bau[47] further derived a closed-form approximation for the dipole coefficient. In Appendix A, we modified the derivation in Zhao and Bau[47] to accommodate the effect of the hydrodynamic slip.

The approximate dipole coefficient accounting for the slip is

$$f_a = -\frac{1}{2} + \frac{1}{6(1+i\lambda_D^2\omega)}\left[\lambda_D + 4Pe\left(\lambda_D^2 + \frac{\beta}{1+3\beta}\lambda_D\right)\right]\zeta^2 + O(\zeta^3). \tag{24}$$

Compared to the dipole coefficient of a nonslip particle, Eq. (24) has an extra term $4Pe\beta\lambda_D\zeta^2/(1+3\beta)$ denoting the contribution of the hydrodynamic slip to the dipole coefficient. Equation (24) indicates that the dipole moment is dominated by the electrophoertic motion. Khair and Squires[37] showed that in the case of thick double layers, the hydrodynamic slip enhances the electrophoretic mobility by simply reducing the viscous drag on the particle. Equation (24) reveals that when $\lambda_D \gg 1$, the hydrodynamic slip leads to an enhancement of the dipole moment just owing to the enhancement of the electrophoretic motion.

To test the range of validity of formula (24), we compare its predictions with numerically calculated values of the dipole coefficient (Sec. III). Figure 3 depicts the dipole coefficient Re(f) as a function of the frequency when $\zeta=-0.2$. Figures 3(a) and 3(b) correspond, respectively, to $\lambda_D=10$ and $\lambda_D=15$. The lines and symbols correspond, respectively, to the predictions of Eq. (24) and numerical results computed with the PNP model. The solid, dashed, and dashed-dotted lines are, respectively, $\beta=0.1$, $\beta=1$, and $\beta=10$. Figure 3 shows excellent agreements between the predictions of the approximate formula (24) and the numerical calculations over a broad range of frequencies.

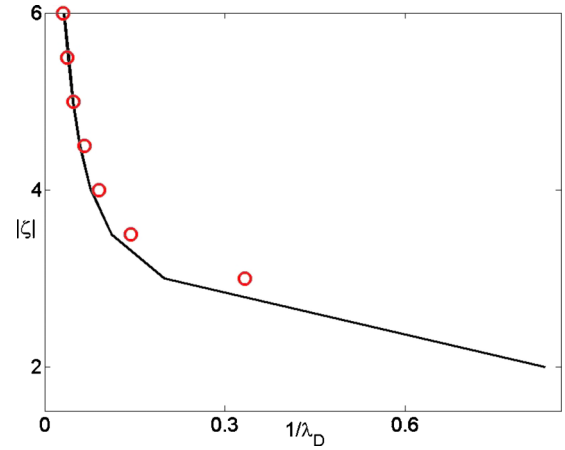

FIG. 4. (Color online) The range of validity of the approximate formula [Eq. (24)] for the dipole coefficient as a function of the zeta (ζ) potential and the electric double layer thickness (λ_D). In the region under the curve, the formula is accurate within better than 5% when $\omega\lambda_D^2<0.1$. The line and symbols are, respectively, $\beta=1$, and $\beta=10$.

Figure 4 depicts the relative error incurred using formula (24) compared to the PNP model's numerical predictions as a function of $|\zeta|$ and λ_D when $\omega\lambda_D^2<0.1$. The space under the curve delineates the region where the relative error is smaller than 5%. The line and symbols correspond, respectively, to $\beta=1$, and $\beta=10$. Figure 4 suggests that the validity of formula (24) is mainly determined by the double layer thickness λ_D and the zeta potential. Interestingly, the influence of the slip length β on the validity is insignificant. Despite the fact that formula (24) is derived in the limit $\lambda_D \gg 1$, Fig. 4 indicates that the approximate dipole coefficient (24) is actually applicable for a much moderate double layer length and zeta potential.

V. THE DIPOLE MOMENT FOR THIN DOUBLE LAYERS

We now turn to the opposite limit of thin double layers $\lambda_D \ll 1$. In contrast to the case of thick double layers, ion transport inside the double layer plays an important role in determining the dipole moment coefficient. At high frequencies, ions' migration and convection are dominant. A surface conduction model can be developed to account for the effects of migration and convection.

A. Surface conduction (MWO) model

When one is studying the dielectric properties of dilute suspensions and calculating dielectrophoretic forces, often the dipole coefficient of a spherical particle is approximated as[40,41]

$$f = \frac{\bar{\varepsilon}_2^* - \bar{\varepsilon}_1^*}{\bar{\varepsilon}_2^* + 2\bar{\varepsilon}_1^*}, \tag{25}$$

where

Downloaded 13 Aug 2013 to 131.216.164.149. This article is copyrighted as indicated in the abstract. Reuse of AIP content is subject to the terms at: http://pof.aip.org/about/rights_and_permissions

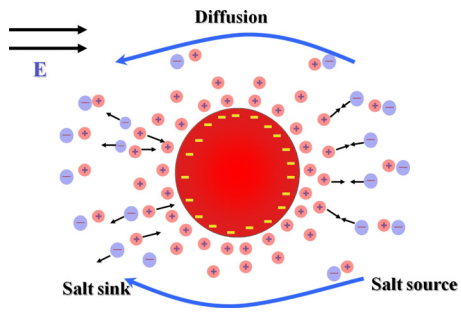

FIG. 5. (Color online) A schematic of the expelling-entraining process which creates bulk concentration gradients.

$$\bar{\varepsilon}_i^* = \varepsilon_i^* - i\frac{\kappa_i^*}{\omega^*}. \tag{26}$$

In the above, $\bar{\varepsilon}_1^*$ and $\bar{\varepsilon}_2^*$ are, respectively, the complex permittivities of the electrolyte and the particle; and κ_1^* and κ_2^* are, respectively, the conductivities of the electrolyte and the particle. The electrolyte's conductivity is given by $\kappa_1^* = 2F_a^{*2}D_+^*C_0^*/R^*T^*$.[43] The particle's effective conductivity is $\kappa_2^* = \kappa_2^{(i)^*} + 2\sigma_s^{(DL)^*}/a^*$, where $\kappa_2^{(i)^*}$ and $\sigma_s^{(DL)^*}$ are, respectively, the intrinsic conductivity of the particle and the surface conductivity of the diffuse layer.[48] Here, we assume that $\kappa_2^{(i)^*} = 0$. When the electric double layer is thin ($\lambda_D \ll 1$),[37]

$$\sigma_s^{(DL)^*} = \left\{ 2\lambda_D^*\left[\cosh\left(\frac{\zeta}{2}\right) - 1\right](1+3m) + 3m\beta^*[\cosh(\zeta) - 1]\right\}\kappa_1^*, \tag{27}$$

where ion mobility m

$$m = \frac{2\varepsilon_1^* R^{*2}T^{*2}}{3F^{*2}\mu^* D_+^*}. \tag{28}$$

In the low-frequency limit ($\omega \to 0$), $f = (\kappa_2^* - \kappa_1^*)/(\kappa_2^* + 2\kappa_1^*) = (2Du-1)/(2Du+2)$, where $Du = \sigma_s^{(DL)^*}/(a^*\kappa_1^*)$ is the Dukhin number.[43] The last term in Eq. (27) represents the contribution to the dipole moment from the slip at the particle surface. Thus as the slip length β^* increases, so does the Dukhin number, leading to a higher dipole coefficient.

B. The low-frequency (Dukhin–Shilov) model

Ions' migration and convection often deplete ions into the bulk at the one side of the particle and withdraw ions from the bulk at the other side, creating a concentration gradient. At low frequencies, ions have sufficient time to diffuse responding to the concentration polarization (Fig. 5). As a result, the process of diffusion modifies the dipole coefficient at low frequencies. However, the MWO model (Sec. V A) does not account for diffusion in the electrolyte solution, is applicable only when $\omega^* \gg D^*/a^{*2}$, and fails to predict the low-frequency dispersion.[46,50,51] To understand the role of the diffusion, Dukhin and Shilov (i.e., see Grosse and Shilov,[53] Zhao and Bau,[51] and Appendix B) used asymptotic analysis to calculate the dipole coefficient in the limit of thin double layers $\lambda_D \ll 1$.

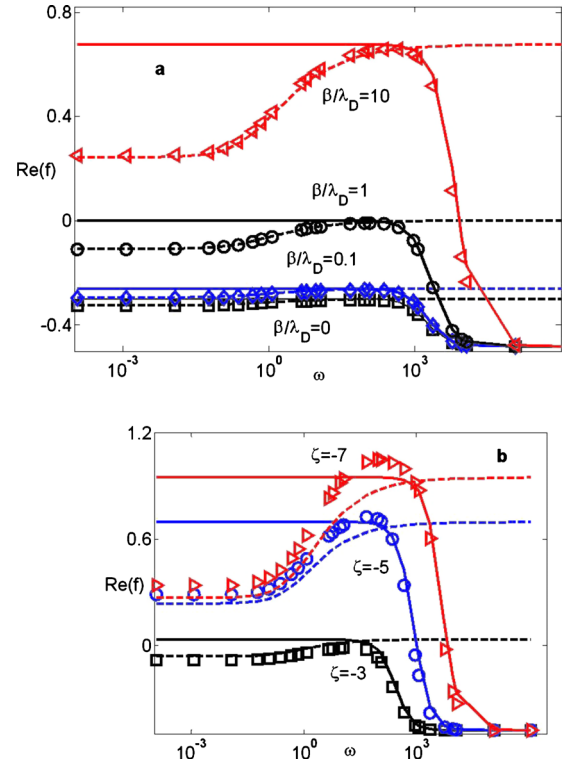

FIG. 6. (Color online) The dipole coefficient Re(f) as a function of the frequency ω. (a) $\lambda_D = 0.01$ and $\zeta = -5$; (b) $\lambda_D = 0.03$ and $\beta = 0.1$. The solid lines, the dashed lines, and the symbols correspond, respectively, to the predictions from the MWO model, the DS model, and the PNP model.

In the thin double layer limit, Grosse and Shilov[53] presented a detailed derivation procedure to calculate the analytical dipole moment for a nonslip, charged, dielectric, spherical particle. In Appendix B, we apply this procedure to account for the hydrodynamic slip. For brevity, we only present the final expression of the dipole coefficient

$$f = f_\infty - K_d H, \tag{29}$$

where detailed expressions of f_∞, K_d, and H are given in Appendix B.

For a nonslip spherical particle ($\beta = 0$), Eq. (29) reduces to the same dipole expression as that in Grosse and Shilov.[53] At high frequencies ($\omega \gg 1$), Eq. (29) can be rewritten as $f = f_\infty = (2Du-1)/(2Du+2)$. Not surprisingly, the high-frequency limit of the DS model is equal to the low-frequency limit of the MWO model.

Figure 6(a) plots the dipole coefficient Re(f) as a function of the frequency ω for a number of slip lengths when $\lambda_D = 0.01$ and $\zeta = -5$. Figure 6(b) depicts the dipole coefficient Re(f) as a function of the frequency ω for a range of zeta potentials where $\lambda_D = 0.03$ and $\beta = 0.1$. The solid lines, the dashed lines, and the symbols correspond, respectively, to the predictions from the MWO model, the DS model, and the PNP model. As expected, the MWO model fails to predict the dipole coefficient at low frequencies where the diffusion is important and the DS model is only valid at low frequencies since the basic assumption that the double layer is at local equilibrium to derive Eq. (29) is not valid at high frequencies. The dipole coefficients predicted from the PNP

Downloaded 13 Aug 2013 to 131.216.164.149. This article is copyrighted as indicated in the abstract. Reuse of AIP content is subject to the terms at: http://pof.aip.org/about/rights_and_permissions

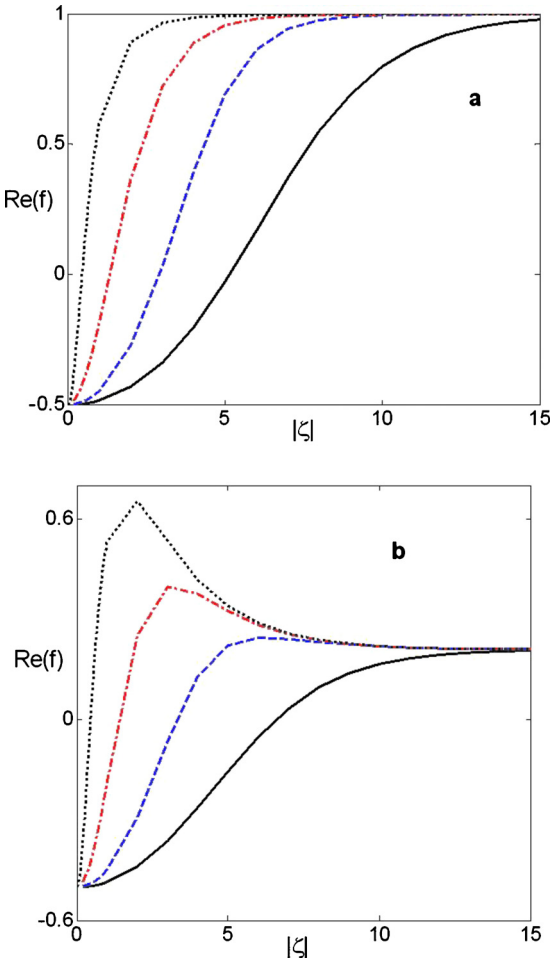

FIG. 7. (Color online) The dipole coefficient Re(f) as a function of the zeta potential ζ. (a) The low-frequency limit of the MWO model and (b) the low-frequency limit of the DS model. The solid, dashed, dashed-dotted, and dotted lines denote, respectively, $\beta=0$, $\beta=0.1$, $\beta=1$, and $\beta=10$.

model agree well, respectively, with those of the MWO model at high frequencies and DS model at low frequencies. Figure 6 also indicates that the slip length has little to do with the validity of the MWO and DS models, which is again dictated by the double layer length and zeta potential.

To study the effect of the hydrodynamic slip on the dipole coefficient, we depict the dipole coefficient as a function of the zeta potential ζ for different slip lengths in Fig. 7. In Fig. 7(a), the low-frequency limit of the MWO model, corresponding to the peak value of the dipole coefficient, is plotted. Meanwhile the low-frequency limit of the DS model is recorded in Fig. 7(b). The solid, dashed, dotted-dashed, and dotted lines denote, respectively, $\beta=0$, $\beta=0.1$, $\beta=1$, and $\beta=10$.

In the absence of the concentration polarization (the low-frequency limit of the MWO model), the dipole moments asymptotically approach the maximum (1), as ζ increases. The larger β is, the smaller ζ is required to approach the asymptotic maximum. In contrast, in the presence of the concentration polarization (the low-frequency limit of the DS model), the dipole coefficient initially increases, attains a maximum, and then asymptotically approaches a constant. Remarkably, at large zeta potentials, the enhancement of the dipole moment due to the hydrodynamic slip disappears and curves corresponding to different β converge.

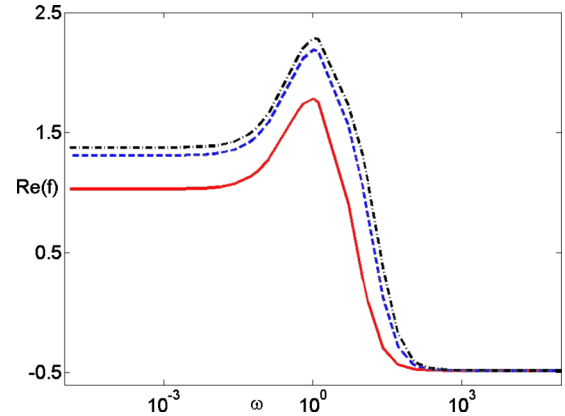

FIG. 8. (Color online) The dipole coefficient Re(f) as a function of the frequency ω when $\lambda_D=0.3$ and $\zeta=-5$. The solid, dashed, and dashed-dotted lines correspond, respectively, to $\beta=0.1$, $\beta=1$, and $\beta=10$.

The different ζ dependences between high frequencies and low frequencies indicate that different underlying mechanisms dominate at different frequency ranges. At high frequencies, the dipole moment is determined by ions' migration and convection. The hydrodynamic slip can significantly boost the induced electro-osmotic flow near a charged surface, which, in turn, enhances the convection. A larger slip length β means a stronger convection or a larger surface conduction. It is not surprising that the dipole moment associated with the large slip length β approaches its maximum more quickly as ζ increases.

However, at low frequencies, the polarization is dictated by the balance of ions' migration, convection, and diffusion. Although a large ζ substantially increases the surface conduction, it also simultaneously creates a stronger concentration gradient. Since the direction of the bulk diffusion is opposite to the direction of the surface conduction, the bulk diffusion counters against the surface conduction, resulting in a reduction of the dipole moment. The interplay between the bulk diffusion and the surface conduction yields to a rather complicated relationship between the dipole coefficient and ζ at low frequencies. At large ζ, the advantage of the hydrodynamic slip on the dipole moment is lost, which can be attributed to the importance of the bulk diffusion at low frequencies. As pointed out by Khair and Squires,[37] the concentration polarization leads to the nonuniform surface conduction at large ζ, also responsible for the loss of the enhancement of the electrophoretic mobility due to the hydrodynamic slip.

VI. THE DIPOLE COEFFICIENT FOR AN ARBITRARY λ_D

For an arbitrary double layer thickness, both the thick-double-layer and the thin-double-layer theories are not applicable. The PNP model in Sec. III has to be solved numerically. Figure 8 depicts the dipole coefficient Re(f) as a function of the frequency ω when $\lambda_D=0.3$ and $\zeta=-5$. The solid, dashed, and dashed-dotted lines correspond, respectively, to $\beta=0.1$, $\beta=1$, and $\beta=10$. Similar to that of a nonslip

Downloaded 13 Aug 2013 to 131.216.164.149. This article is copyrighted as indicated in the abstract. Reuse of AIP content is subject to the terms at: http://pof.aip.org/about/rights_and_permissions

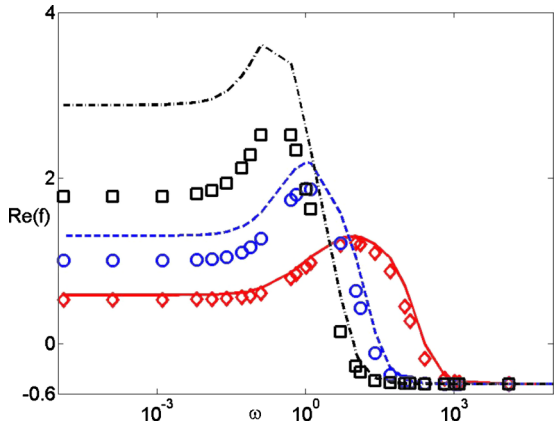

FIG. 9. (Color online) The dipole coefficient Re(f) (lines) and the dipole coefficient Re(f^E) (symbols) neglecting the contribution from the particle's electrophoretic motion as functions of the frequency ω when $\beta=1$ and $\zeta=-5$. The solid line (diamonds), the dashed line (circles), and the dashed-dotted lines (squares) correspond, respectively, to $\lambda_D=0.1$, $\lambda_D=0.3$, and $\lambda_D=0.6$

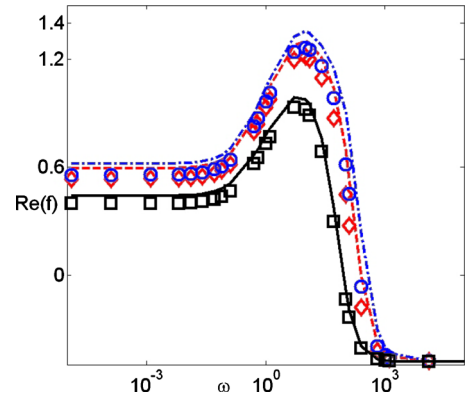

FIG. 10. (Color online) The dipole coefficient Re(f) (lines) and the dipole coefficient Re(f^E) (symbols) neglecting the contribution from the particle's electrophoretic motion as functions of the frequency ω when $\lambda_D=0.1$ and $\zeta=-5$. The solid line (squares), the dashed line (circles), and the dashed-dotted lines (diamonds) correspond, respectively, to $\beta=0.1$, $\beta=1$, and $\beta=10$.

spherical particle, the dipole coefficient arises, reaches a peak value, and then decreases to a constant value as the frequency decreases. The dipole coefficient exhibits both high-frequency and low-frequency dispersions. When the frequency is high, ion finite mobility prevents ions from responding to the applied electric field and the polarization is dominated by the mismatch of the dielectric permittivity between the particle and the electrolyte. Since the particle's dielectric permittivity is much smaller than that of the electrolyte, the dipole coefficient is negative or the particle experiences negative DEP. As the frequency decreases, ions inside the double layer have time to migrate under the influence of the applied electric field and ions' migration and convection consist of ionic current along the particle's surface, which begins to exceed the influence of dielectric permittivity. Accordingly, the dipole moment arises. In particular, when the ionic current from migration and convection is larger than the bulk conductivity of the medium, the dipole moment changes the sign, becomes positive, and the particle exhibits positive DEP. When the frequency is around D^*/a^{*2}, the process of the bulk diffusion, opposite to the direction of the surface conduction, leads to a reduction of the dipole moment. When the frequency further decreases, the diffusion also reaches its equilibrium and the dipole coefficient becomes independent of the frequency and is dictated by the balance of the surface conduction and bulk diffusion.

Figure 8 indicates that the hydrodynamic slip not only enhances the dipole moment by inducing a stronger electroosmotic flow, but also shifts the critical frequency of the high-frequency dispersion which corresponds to the case that the dipole coefficient is equal to zero. Since the high-frequency dispersion is governed by the mismatch between the surface conduction and the bulk conduction, the hydrodynamic slip effectively increases the surface conduction, shifting the critical frequency to a higher value. On the contrary, the low-frequency dispersion is governed by the diffusion whose time scale is around a^{*2}/D^*. The hydrodynamic slip only impacts the magnitude of the dipole moment but does not modify the diffusion time. Thus, the low-frequency dispersions with different hydrodynamic slip lengths β are the same (D^*/a^{*2}). In other words, the hydrodynamic slip only affects the time scale associated with the surface conduction and has little impact on the diffusion time scale.

To study the importance of the electrophoretic motion on the dipole moment, Fig. 9 plots the dipole coefficient Re(f) (lines) and the dipole coefficient Re(f^E) (symbols), neglecting the contribution from the particle's electrophoretic motion as functions of the frequency ω when $\beta=1$ and $\zeta=-5$. The solid line (diamonds), the dashed line (circles), and the dashed-dotted lines (squares) correspond, respectively, to $\lambda_D=0.1$, $\lambda_D=0.3$, and $\lambda_D=0.6$. Consistent with the conclusion of Grosse *et al.*,[43] the dipole moment deviates from Re(f^E) when $\lambda_D>0.1$. In other words, the contribution of particle's electrophoretic motion to the dipole moment has to be taken into account to accurately predict the particle's dielectrophoretic motion when the double layer length is not small. Indeed, the approximate expression of the dipole moment in Sec. IV concludes that the contribution from the electrophoretic motion is the leading order in the limit of thick double layers.

Furthermore, Fig. 10 depicts the dipole coefficient Re(f) (lines) and the dipole coefficient Re(f^E) (symbols) as functions of the frequency ω when $\lambda_D=0.1$ and $\zeta=-5$. The solid line (squares), the dashed line (circles), and the dashed-dotted line (diamonds) denote, respectively, $\beta=0.1$, $\beta=1$, and $\beta=10$. Figure 10 reveals that the slip length has little impact on the importance of the electrophoretic motion, which is rather determined by the double layer thickness.

Figure 11 plots the dipole coefficient as a function of the slip length β when $\zeta=-5$ and $\omega=10^{-4}$. The solid and dashed lines denote, respectively, $\lambda_D=0.1$ and $\lambda_D=0.3$. The dipole moment quickly arises and then exponentially approaches a constant as the slip length β increases. Since only ions' migration and convection inside the double layer affect the dipole moment, it is not surprising that when the slip length is much larger than the double layer thickness further increase of the slip length has almost no effect on the dipole moment.

Downloaded 13 Aug 2013 to 131.216.164.149. This article is copyrighted as indicated in the abstract. Reuse of AIP content is subject to the terms at: http://pof.aip.org/about/rights_and_permissions

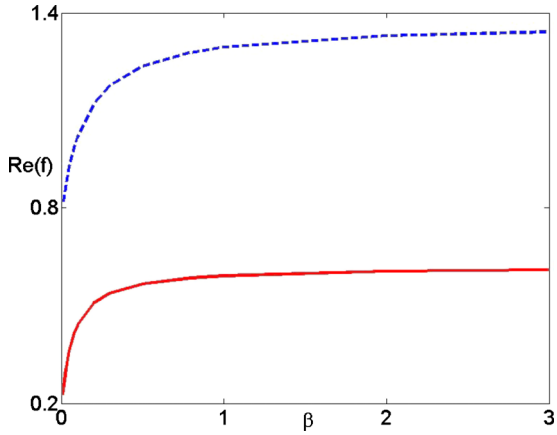

FIG. 11. (Color online) The dipole coefficient Re(f) as a function of the slip length β when $\zeta=-5$ and $\omega=10^{-4}$. The solid and dashed lines denote, respectively, $\lambda_D=0.1$ and $\lambda_D=0.3$.

Finally, in Fig. 12, we plot the dipole coefficient Re(f) as a function of the zeta potential ζ when $\omega=10^{-4}$. (a) $\lambda_D=0.1$; (b) $\lambda_D=0.3$; (c) $\lambda_D=1$; and (d) $\lambda_D=10$. The solid, the dashed, and the dashed-dotted lines correspond, respectively, to $\beta=0.1$, $\beta=1$, and $\beta=10$. Similar to that predicted by the DS model, when $\lambda_D<1$, the dipole coefficient increases, reaches a peak value, and then decreases as the zeta potential increases. Similarly the enhancement caused by the hydrodynamic slip is lost at large zeta potentials. On the contrary, in the case of large double layers ($\lambda_D>1$), the dipole coefficient asymptotically increases with the zeta potential. Interestingly, the enhancement, due to the hydrodynamic slip, though weak, still exists at relatively large zeta potentials. It is readily explained: when $\lambda_D>1$, the dipole moment is dominated by the electrophoretic motion and the electrophoretic mobility increases asymptotically as the zeta potential increases in the case of $\lambda_D>1$. Thus, so does the dipole moment.

VII. CONCLUSION

In this article, inspired by recent experimental works[15–25] and theoretical predictions[33–37] of the enhancement of osmotic flows and phoretic velocities due to the hydrodynamic slip, we computed the dipole coefficient of a charged dielectric, spherical, particle with the hydrodynamic slipping surface as a function of the frequency, the double layer length, zeta potential, and the slip length using the standard Poisson–Nernst–Planck equations. Our aim was on the influence of the hydrodynamic slip on the particle's polarization. We observed that the slip not only changed the magnitude of the dipole moment coefficient, but also increased the critical frequency where the dipole moment of a particle is equal to zero. The dependence of the critical frequency of the high-frequency dispersion on the slip length might suggest the possibility of separating particles among their surface hydrodynamic properties. For example, at certain frequency, particles with small slip lengths (negative DEP) will be repelled from the location of the electric field maximum, while particles with large slip lengths (positive DEP) will be attracted to the location of the electric field maximum.

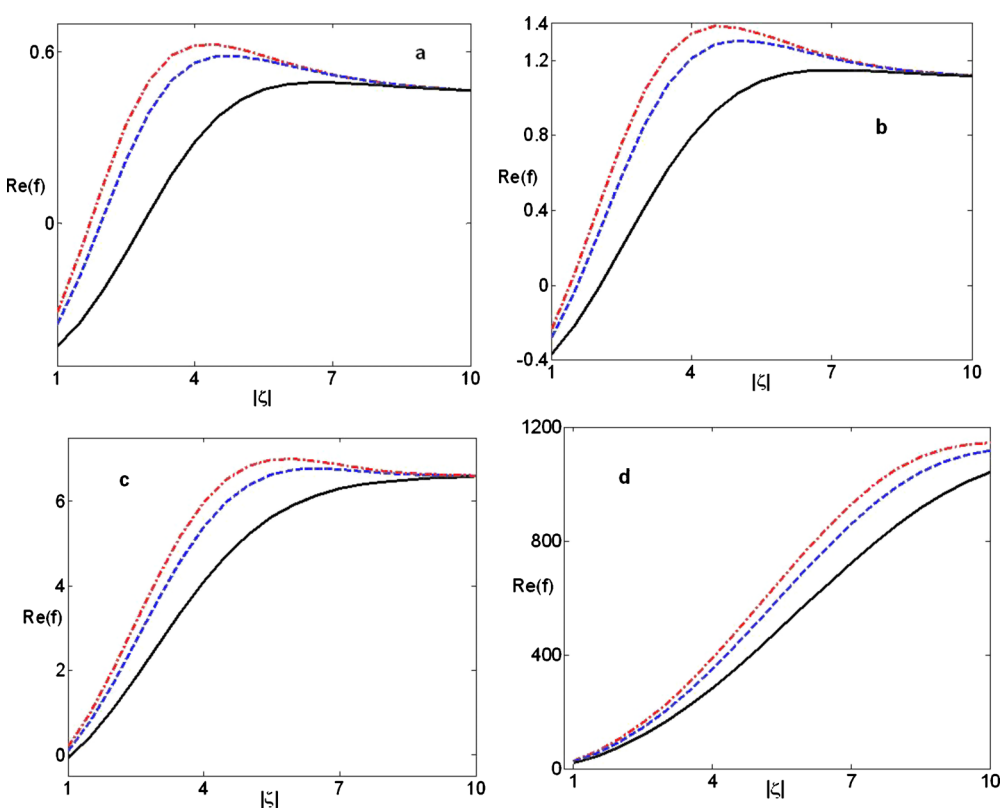

FIG. 12. (Color online) The dipole coefficient Re(f) as a function of the zeta potential ζ when $\omega=10^{-4}$. (a) $\lambda_D=0.1$; (b) $\lambda_D=0.3$; (c) $\lambda_D=1$; and (d) $\lambda_D=10$. The solid, the dashed, and the dashed-dotted lines correspond, respectively, to $\beta=0.1$, $\beta=1$, and $\beta=10$.

Downloaded 13 Aug 2013 to 131.216.164.149. This article is copyrighted as indicated in the abstract. Reuse of AIP content is subject to the terms at: http://pof.aip.org/about/rights_and_permissions

Using a perturbation expansion, in the case of small zeta potentials and thick double layers ($\lambda_D \gg 1$), a simple approximate expression for the dipole coefficient was derived. It concluded that for large double layers, the increase of the dipole coefficient was simply attributed to the enhancement of the electrophoretic mobility of the particle boosted by the hydrodynamic slip.

In contrast, for thin double layers ($\lambda_D \ll 1$), the polarization of the spherical particle was dominated by ion transport inside the double layer and the contribution from the electrophoretic motion is negligible. In this case, the dipole moment coefficient can be expressed by the MWO model at high frequencies and the DS model at low frequencies. We found out that the hydrodynamic slip can effectively enhance ions' convection inside the double layer and thereafter increase the surface conduction, leading to a higher dipole moment coefficient. However, at low frequencies, the bulk diffusion complicated the process. The hydrodynamic slip increases the dipole moment at small and moderate zeta potentials. At large zeta potentials, the advantage of the slip is lost and the dipole moment is independent of the slip length. This loss is due to the importance of the bulk diffusion at low frequencies also enhanced by the slip, which counters against the surface conduction.

For an arbitrary double layer thickness, we solved the PNP model numerically to bridge the simple theories of large double layers and thin double layers. We revealed that as the double layer length increases, so does the importance of the contribution from the particle's electrophoertic motion to the dipole moment. Interestingly, the enhancement at high zeta potentials, which is lost in the case of thin double layers, appears again.

ACKNOWLEDGMENTS

This work was supported, in part, by UNLV Start-up Fund.

APPENDIX A: THE DIPOLE MOMENT FOR THICK DOUBLE LAYERS AND SMALL ZETA POTENTIALS WITH THE SLIP

Zhao and Bau[47] derived an approximate expression for the dipole moment of a weakly charged, spherical particle with a small dielectric constant and thick double layer ($\lambda_D \gg 1$). In this appendix, we modify the derivation to accommodate the effect of the hydrodynamic slip.

Under the assumption of $\zeta \ll 1$, we can further expand all the perturbed variables into power series in terms of ζ For example,

$$\varphi^{(1)} = \varphi^{(1),[0]} + \varphi^{(1),[1]}\zeta + \varphi^{(1),[2]}\zeta^2 + O(\zeta^3), \tag{A1}$$

$$C_{\pm}^{(1)} = C_{\pm}^{(1),[0]} + C_{\pm}^{(1),[1]}\zeta + C_{\pm}^{(1),[2]}\zeta^2 + O(\zeta^3), \tag{A2}$$

$$\vec{u}^{(1)} = \vec{u}^{(1),[0]} + \vec{u}^{(1),[1]}\zeta + \vec{u}^{(1),[2]}\zeta^2 + O(\zeta^3), \tag{A3}$$

and accordingly the dipole moment expression is

$$f = f^{[0]} + f^{[1]}\zeta + f^{[2]}\zeta^2 + O(\zeta^3). \tag{A4}$$

In the above, the superscript $[k]$ denotes the kth order term in the ζ expansion.

When $\zeta \ll 1$, the Debye–Huckel approximation applies and Eq. (12) can be integrated[43]

$$\varphi_1^{(0)} = \frac{\zeta}{r} e^{(1-r)/\lambda_D} \equiv \varphi_1^{(0),[1]}\zeta. \tag{A5}$$

Accordingly, the equilibrium concentrations $C_{\pm}^{(0)}$ become

$$C_{\pm}^{(0)} = e^{\mp\varphi_1^{(0)}} = 1 \mp \varphi_1^{(0),[1]}\zeta + \tfrac{1}{2}(\varphi_1^{(0),[1]})^2\zeta^2 + O(\zeta^3). \tag{A6}$$

The electric charge density is

$$\rho^{(j)} = C_+^{(j)} - C_-^{(j)} = \rho^{(j),[0]} + \rho^{(j),[1]}\zeta + \rho^{(j),[2]}\zeta^2 + O(\zeta^3) \tag{A7}$$

and the average concentration is

$$C^{(j)} = \frac{C_+^{(j)} + C_-^{(j)}}{2} = C^{(j),[0]} + C^{(j),[1]}\zeta + C^{(j),[2]}\zeta^2 + O(\zeta^3). \tag{A8}$$

By adding and subtracting the Nernst–Planck equations (19) for the cations and anions, we have

$$i\omega\rho^{(1)} + \nabla\cdot(-\nabla\rho^{(1)} - 2(C^{(0)}\nabla\varphi_1^{(1)} + C^{(1)}\nabla\varphi_1^{(0)}) + Pe\rho^{(0)}\vec{u}^{(1)}) = 0 \tag{A9}$$

and

$$i\omega C^{(1)} + \nabla\cdot\left[-\nabla C^{(1)} - \tfrac{1}{2}(\rho^{(0)}\nabla\varphi_1^{(1)} + \rho^{(1)}\nabla\varphi_1^{(0)}) + PeC^{(0)}\vec{u}^{(1)}\right] = 0. \tag{A10}$$

In the case of $\varepsilon_r \ll 1$ (a particle with a small dielectric permittivity), the boundary conditions at the particle's surface are

$$\frac{\partial\varphi_1^{(1)[k]}}{\partial n} = \frac{\partial C^{(1)[k]}}{\partial n} = \frac{\partial\rho^{(1)[k]}}{\partial n} = 0 \quad \text{at} \quad r = 1. \tag{A11}$$

Similarly, accounting for the linearity, the original problem can be decoupled into the **E** problem and the **U** problem.

Because the **E** problem, consisting of a stationary particle subjected to a uniform electric field, is identical to that of the nonslip spherical particle which is well documented in Zhao and Bau,[47] the details of the solution process are referred to Zhao and Bau.[47]

The **U** problem consists of a weakly charged, stationary particle whose surface experiences hydrodynamic slip, subjected to a uniform flow field (U_0). When $\lambda_D \to \infty$, the electric body force $[O(1/(2\lambda_D^2))]$ in the Stokes equation can be neglected in the absence of the applied electric field and the velocity can be expressed as[80]

$$\vec{u} = U_0\left[1 - \frac{3(1+2\beta)}{2(1+3\beta)r} + \frac{1}{2(1+3\beta)r^3}\right]\cos\theta e_r - U_0\left[1 - \frac{3(1+2\beta)}{4(1+3\beta)r} - \frac{1}{4r^3}\right]\sin\theta e_\theta. \tag{A12}$$

In the above, $U_0 = 2/3(1+3\beta)/(1+2\beta)\zeta$ is the particle's elec-

Downloaded 13 Aug 2013 to 131.216.164.149. This article is copyrighted as indicated in the abstract. Reuse of AIP content is subject to the terms at: http://pof.aip.org/about/rights_and_permissions

trophoretic velocity in the case of thick electric double layers.[37]

The leading order terms in **U** problem are of the second order. $\rho^{(1),[2]}$ satisfies

$$i\omega\rho^{(1),[2]} - \nabla^2\rho^{(1),[2]} - 2\nabla^2\varphi_1^{(1),[2]} = -Pe\frac{4}{3}\frac{1+3\beta}{1+2\beta}\left[1 - \frac{3(1+2\beta)}{2(1+3\beta)r} + \frac{1}{2(1+3\beta)r^3}\right]\frac{d\hat{\varphi}_1^{(0),[1]}}{dr}\cos\theta, \tag{A13}$$

and $\varphi_1^{(1),[2]}$ obeys the Poisson equation

$$\nabla^2\varphi_1^{(1),[2]} = -\frac{\rho^{(1),[2]}}{2\lambda_D^2}. \tag{A14}$$

By substituting Eq. (A14) into Eq. (A13), we have

$$-\nabla^2[2(i\omega\lambda_D^2+1)\varphi_1^{(1),[2]} + \rho^{(1),[2]}] = -Pe\frac{4}{3}\frac{1+3\beta}{1+2\beta}\left[1 - \frac{3(1+2\beta)}{2(1+3\beta)r} + \frac{1}{2(1+3\beta)r^3}\right]\frac{d\hat{\varphi}_1^{(0),[1]}}{dr}\cos\theta, \tag{A15}$$

with the boundary conditions

$$\rho^{(1),[2]} = 0, \quad \text{and} \quad \varphi_1^{(1),[2]} = 0, \quad \text{at } r \to \infty. \tag{A16}$$

The solution of Eq. (A15) admits the form

$$[(2i\omega\lambda_D^2+2)\varphi_1^{(1),[2]} + \rho^{(1),[2]}] = \left[\frac{B}{r^2} + F(r)\right]\cos\theta. \tag{A17}$$

Since the right hand side of Eq. (A15) is proportional to $e^{(1-r)/\lambda_D}$, $F(r)$ decays exponentially with r. With the aid of the Poisson equation, we replace the electric charge in Eq. (A17) with the potential to obtain

$$\nabla^2\varphi_1^{(1),[2]} - \left(i\omega + \frac{1}{\lambda_D^2}\right)\varphi_1^{(1),[2]} = -\frac{1}{2\lambda_D^2}\left[\frac{B}{r^2} + F(r)\right]\cos\theta. \tag{A18}$$

Considering that the dipole moment is estimated from the far field electric potential, we deduce from Eq. (A18)

$$f^{[2]} = \frac{B}{2(1+i\lambda_D^2\omega)}. \tag{A19}$$

To calculate B, we need to solve Eq. (A15). The solution of Eq. (A15) can be written in terms of a Green function.[79]

$$[(2i\omega\lambda_D^2+2)\hat{\varphi}_1^{(1),[2]} + \hat{\rho}^{(1),[2]}] = -\frac{1}{3r^2}\int_1^r\left(x^3+\frac{1}{2}\right)\hat{G}(x)dx - \frac{1}{3}\left(r+\frac{1}{2r^2}\right)\int_r^\infty \hat{G}(x)dx, \tag{A20}$$

where the variables with the hat $\hat{A}(r)$ are functions of r only $[A(r,\theta)=\hat{A}(r)\cos\theta]$ and

$$\hat{G}(x) = -Pe\frac{4}{3}\left(\frac{1+3\beta}{1+2\beta}\right)\times\left[1 - \frac{3(1+2\beta)}{2(1+3\beta)x} + \frac{1}{2(1+3L_s)x^3}\right]\frac{d\hat{\varphi}_1^{(0),[1]}}{dx}. \tag{A21}$$

When $r\to\infty$, we deduce $[(2i\omega\lambda_D^2+2)\hat{\varphi}_1^{(1),[2]}+\hat{\rho}^{(1),[2]}]r^2 \sim B$. Thus from Eq. (A20),

$$B = -\frac{1}{3}\int_1^\infty\left(x^3+\frac{1}{2}\right)\hat{G}(x)dx. \tag{A22}$$

Integrating Eq. (A22) with $\hat{G}(x)$ given in Eq. (A21), we can further expand the solution of B in terms of a series of λ_D and let $\lambda_D\to\infty$. We have

$$B = \frac{4Pe}{3}\left[\lambda_D^2 + \frac{\beta}{1+3\beta}\lambda_D + O(1)\right]\zeta^2 + O(\zeta^3). \tag{A23}$$

Therefore, the contribution of the particle's electrophoretic motion to the dipole moment $U_0 f^U$ is:

$$U_0 f^U = \frac{2Pe}{3(1+i\lambda_D^2\omega)}\left(\lambda_D^2 + \frac{\beta}{1+3\beta}\lambda_D\right)\zeta^2 + O(\zeta^3). \tag{A24}$$

APPENDIX B: THE LOW-FREQUENCY THEORY ACCOUNTING FOR THE SLIP FOR THIN DOUBLE LAYERS

In this appendix, we modify the low-frequency theory of a nonslip, charged, dielectric, spherical particle in the limit of thin double layers ($\lambda_D \ll 1$) (Ref. 53) to include the influence of the hydrodynamic slip.

Following the procedure outlined in Grosse and Shilov,[53] we define the dimensionless electrochemical potential as

$$\mu_\pm = \ln C_\pm \pm \varphi. \tag{B1}$$

When the applied electric field is weak, the electrochemical potential can be expanded in terms of the external electric field as in Sec. III.

$$\mu_\pm = \mu_\pm^{(0)} + \delta\mu_\pm^{(1)} + O(\delta^2), \tag{B2}$$

where

$$\mu_\pm^{(1)} = C_\pm^{(1)} \pm \varphi^{(1)}. \tag{B3}$$

Now we introduce an analog, neutral, virtual system ($\tilde{n}=\tilde{C}_+=\tilde{C}_-, \tilde{\varphi}$) that is in local equilibrium with the real system. The equivalent system is defined through the mapping

$$\ln(C_\pm^{(1)}) \pm \varphi^{(1)} = \ln(\tilde{n}) \pm \tilde{\varphi}, \tag{B4}$$

where $\tilde{n}$ and $\tilde{\varphi}$ are, respectively, the solute concentration and the electric potential of the virtual system.

In the absence of an external electric field, the system is in equilibrium and the left hand side of Eq. (B4) is equal to zero, and the solutions of Eq. (B4) are $\tilde{n}=1$ and $\tilde{\varphi}=0$.

Further, $\tilde{n}$ can be expanded in terms of the external electric field in the presence of the applied field.

Downloaded 13 Aug 2013 to 131.216.164.149. This article is copyrighted as indicated in the abstract. Reuse of AIP content is subject to the terms at: http://pof.aip.org/about/rights_and_permissions

$$\tilde{n} = 1 + \delta\tilde{n}^{(1)} + O(\delta^2). \tag{B5}$$

Neglecting higher order terms, we use Eq. (B4) to express $\tilde{n}^{(1)}$ and $\tilde{\varphi}^{(1)}$ in terms of $C_{\pm}^{(1)}$ and $\varphi^{(1)}$.

$$\tilde{n}^{(1)} = \frac{1}{2}\left(\frac{C_+^{(1)}}{C_+^{(0)}} + \frac{C_-^{(1)}}{C_-^{(0)}}\right). \tag{B6}$$

$$\tilde{\varphi}^{(1)} = \varphi^{(1)} + \frac{1}{2}\left(\frac{C_+^{(1)}}{C_+^{(0)}} - \frac{C_-^{(1)}}{C_-^{(0)}}\right). \tag{B7}$$

Or $C_{\pm}^{(1)}$ can be expressed in terms of $\tilde{n}^{(1)}$ and $\tilde{\varphi}^{(1)}$.

$$C_{\pm}^{(1)} = C_{\pm}^{(0)}(\tilde{n}^{(1)} \pm \tilde{\varphi}^{(1)} \mp \varphi^{(1)}). \tag{B8}$$

$$\mu_{\pm}^{(1)} = \tilde{n}^{(1)} \pm \tilde{\varphi}^{(1)}. \tag{B9}$$

Next, rewriting the Nernst–Planck and the Poisson equations in terms of the chemical potential and introducing the virtual system's variables, we have

$$\nabla^2\tilde{n}^{(1)} = \nabla\varphi^{(0)} \cdot \nabla\tilde{\varphi}^{(1)} + i\omega\tilde{n}^{(1)} \tag{B10}$$

and

$$\nabla^2\tilde{\varphi}^{(1)} = \nabla\varphi^{(0)} \cdot \nabla\tilde{n}^{(1)} - \nabla\varphi^{(0)} \cdot \vec{u}^{(1)} + i\omega(\tilde{\varphi}^{(1)} - \varphi^{(1)}). \tag{B11}$$

Outside the electric double layer, $\varphi^{(0)}=0$ and the electrical neutrality requires $\tilde{\varphi}^{(1)}=\varphi^{(1)}$. Hence, Eqs. (B10) and (B11) can be readily solved outside the electric double layer.[53]

$$\tilde{n}^{(1)} = K_c\frac{e^{-(1+i)W(r-1)}}{r^2}\frac{1+(1+i)Wr}{1+W+iW}\cos\theta, \tag{B12}$$

$$\tilde{\varphi}^{(1)} = \left(-r + \frac{f}{r^2}\right)\cos\theta. \tag{B13}$$

In the above, $W=\sqrt{\omega/2}$. K_c and f (the dipole coefficient) are integration constants that still need to be determined.

With respect to the boundary conditions on the surface of the particle, we omit the details of the derivation and refer interested readers to Grosse and Shilov.[53] Briefly, assuming a thin electric double layer in local equilibrium (i.e., the chemical potential in the electric double layer is independent of the radial coordinate), we write down the species conservation equations in terms of the actual and far field variables, take the difference, and integrate the resulting equation in terms of the radial coordinate from $r=1$ to infinity to obtain the boundary conditions

$$\left.\frac{\partial\mu_{\pm}^{(1)}}{\partial r}\right|_{r=1} = -\frac{\partial}{\partial\theta}\left[G_{\pm}^{(0)}\left(\frac{\partial\mu_{\pm}^{(1)}}{\partial\theta}\right)_{r=1} + \int_1^{\infty}(1-C_{\pm}^{(0)})u_{\theta}^{(1)}dr\right], \tag{B14}$$

where $G_{\pm}^{(0)}=\int_1^{\infty}(C_{\pm}^{(0)}-1)dr$. In the limit of a thin electric double layer, the surface is assumed to be flat, which allows one to evaluate $G_{\pm}^{(0)}$ and the velocity $u_{\theta}^{(1)}$ in closed form. The tangential velocity $u_{\theta}^{(1)}$, accounting for the influence of the hydrodynamic slip, can be written as[37]

$$u_{\theta}^{(1)} = \zeta\frac{\partial\tilde{\varphi}^{(1)}}{\partial\theta} - 4\ln\left[\cosh\left(\frac{\zeta}{4}\right)\right]\frac{\partial\tilde{n}^{(1)}}{\partial\theta} - \frac{\beta}{\lambda_D}\left[(e^{-\zeta/2}-1)\frac{\partial\mu_+^{(1)}}{\partial\theta} + (e^{\zeta/2}-1)\frac{\partial\mu_-^{(1)}}{\partial\theta}\right]. \tag{B15}$$

Notice that the last term in Eq. (B15) denotes the contribution to the electro-osmotic velocity from the hydrodynamic slip. By substituting the expressions that correspond to the various variables outside the electric double layer, we obtain K_c and f.

The dipole coefficient is

$$f = f_{\infty} - K_d H, \tag{B16}$$

where

$$f_{\infty} = \frac{R^+ + R^- - 2 + 3\beta(K^+ - K^-)^2}{R^+ + R^- + 4 + 3\beta(K^+ - K^-)^2} = \frac{2Du - 1}{2Du + 2}. \tag{B17}$$

In the above, we used the identity $R^+ + R^- + 3\beta(K^+ - K^-)^2 = 4Du$.

Further,

$$K_d = \frac{3[(R^+ - R^-) + 3\beta(K^{+2} - K^{-2})]}{2}\frac{1 + W + Wi}{iW^2[A + 3\beta(K^+ - K^-)^2] + (1 + W + Wi)(B + 3/2\beta C)}, \tag{B18}$$

$$H = \frac{R^+ - R^- + 3\beta(K^{+2} - K^{-2})}{R^+ + R^- + 4 + 3\beta(K^+ - K^-)^2}, \tag{B19}$$

$$A = R^+ + R^- + 4, \tag{B20}$$

$$B = (R^+ + 2)(R^- + 2) - 2U - \frac{U}{2}(R^+ + R^-), \tag{B21}$$

$$C = [(4 + 2R^- - U)K^{+2} + (4 + 2R^+ - U)K^{-2} + 2UK^+K^-], \tag{B22}$$

$$R^{\pm} = \lambda_D(4(1 + 3m)(e^{\mp\zeta/2} - 1) \pm 6m\zeta), \tag{B23}$$

$$K^{\pm} = \sqrt{2m}(e^{\mp\zeta/2} - 1), \tag{B24}$$

Downloaded 13 Aug 2013 to 131.216.164.149. This article is copyrighted as indicated in the abstract. Reuse of AIP content is subject to the terms at: http://pof.aip.org/about/rights_and_permissions

$$U = 48m\lambda_D \ln(\cosh \zeta/4), \tag{B25}$$

and

$$W = \sqrt{\frac{\omega}{2}}. \tag{B26}$$

[1] O. D. Velev and S. Gupta, "Materials fabricated by micro and nanoparticle assembly: The challenging path from science to engineering," Adv. Mater. **21**, 1897 (2009).
[2] I. Ermolina and H. Morgan, "The electrokinetic properties of latex particles: Comparison of electrophoresis and dielectrophoresis," J. Colloid Interface Sci. **285**, 419 (2005).
[3] M. Riegelman, H. Liu, and H. H. Bau, "Controlled nanoassembly and construction of nanofluidic devices," ASME Trans. J. Fluids Eng. **128**, 6 (2006).
[4] B. H. Lapizco-Encinas and M. R. Rito-Palomares, "Dielectrophoresis for the manipulation of nanobioparticles," Electrophoresis **28**, 4521 (2007).
[5] H. Morgan, M. P. Hughes, and N. G. Green, "Separation of submicron bioparticles by dielectrophoresis," Biophys. J. **77**, 516 (1999).
[6] M. E. Arsenault, H. Zhao, P. K. Purohit, Y. E. Goldman, and H. H. Bau, "Confinement and manipulation of actin filaments by electric fields," Biophys. J. **93**, L42 (2007).
[7] M. Z. Bazant and Y. X. Ben, "Theoretical prediction of fast 3D AC electro-osmotic pumps," Lab Chip **6**, 1455 (2006).
[8] J. P. Urbanski, T. Thorsen, J. A. Levitan, and M. Z. Bazant, "Fast ac electro-osmotic micropumps with nonplanar electrodes," Appl. Phys. Lett. **89**, 143508 (2006).
[9] J. P. Urbanski, J. A. Levitan, D. N. Burch, T. Thorsen, and M. Z. Bazant, "The effect of step height on the performance of three-dimensional ac electro-osmotic microfluidic pumps," J. Colloid Interface Sci. **309**, 332 (2007).
[10] H. Zhao and H. H. Bau, "A microfluidic chaotic stirrer utilizing induced-charge electro-osmosis," Phys. Rev. E **75**, 066217 (2007).
[11] T. M. Squires and S. Quake, "Microfluidics: Fluid physics at the nanoliter scale," Rev. Mod. Phys. **77**, 977 (2005).
[12] B. R. Saunders and M. J. Turner, "Nanoparticle-polymer photovoltaic cells," Adv. Colloid Interface Sci. **138**, 1 (2008).
[13] A. Singh, X. Li, V. Protasenko, G. Galantai, M. Kuno, H. Xing, and D. Jena, "Polarization-sensitive nanowire photodetectors based on solution-synthesized CdSe quantum-wire solids," Nano Lett. **7**, 2999 (2007).
[14] O. D. Velev and E. W. Kaler, "In situ assembly of colloidal particles into miniaturized biosensors," Langmuir **15**, 3693 (1999).
[15] C. Neto, D. R. Evans, E. Bonaccurso, H. J. Butt, and V. S. J. Craig, "Boundary slip in Newtonian liquids: A review of experimental studies," Rep. Prog. Phys. **68**, 2859 (2005).
[16] E. Lauga, M. P. Brenner, and H. A. Stone, in *Handbook of Experimental Fluid Dynamics*, edited by C. Tropea, A. Yarin, and J. F. Foss (Springer, New York, 2007), pp. 1219–1240.
[17] O. Vinogradova, "Slippage of water over hydrophobic surfaces," Int. J. Min. Process. **56**, 31 (1999).
[18] U. Ulmanella and C. M. Ho, "Molecular effects on boundary condition in micro/nanoliquid flows," Phys. Fluids **20**, 101512 (2008).
[19] D. Lasne, A. Maali, Y. Amarouchene, L. Cognet, B. Lounis, and H. Kellay, "Velocity profiles of water flowing past solid glass surfaces using fluorescent nanoparticles and molecules as velocity probes," Phys. Rev. Lett. **100**, 214502 (2008).
[20] A. Maali and B. Bhushan, "Slip-length measurement of confined air flow using dynamic atomic force microscopy," Phys. Rev. E **78**, 027302 (2008).
[21] Y. Wang, B. Bhushan, and A. Maali, "Atomic force microscopy measurement of boundary slip on hydrophilic, hydrophobic, and superhydrophobic surfaces," J. Vac. Sci. Technol. A **27**, 754 (2009).
[22] V. M. Muller, I. P. Sergeeva, V. D. Sobolev, and N. V. Churaev, "Boundary effects in the theory of electrokinatic phenomena," Colloid J. USSR **48**, 606 (1986).
[23] L. Joly, C. Ybert, E. Trizac, and L. Bocquet, "Hydrodynamics within the electric double layer on slipping surfaces," Phys. Rev. Lett. **93**, 257805 (2004).
[24] N. V. Churaev, J. Ralston, I. P. Sergeeva, and V. D. Sobolev, "Electrokientic properties of methylated quartz capillaries," Adv. Colloid Interface Sci. **96**, 265 (2002).
[25] C. I. Bouzigues, P. Tabeling, and L. Bocquet, "Nanofluidics in the Debye layer at hydrophilic and hydrophobic surfaces," Phys. Rev. Lett. **101**, 114503 (2008).
[26] K. Ichiki, A. E. Kobryn, and A. Kovalenko, "Targeting transport properties in nanofluidics: Hydrodynamic interaction among slip surface nanoparticles in solution," J. Comput. Theor. Nanosci. **5**, 2004 (2008).
[27] N. J. Shirtcliffe, G. McHale, M. I. Newton, and Y. Zhang, "Superhydrophobic copper tubes with possible flow enhancement and drag reduction," ACS Appl. Mater. Interfaces **1**, 1316 (2009).
[28] Y. Ren and D. Stein, "Slip-enhanced electrokinetic energy conversion in nanofluidic channels," Nanotechnology **19**, 195707 (2008).
[29] S. Pennathur, J. C. T. Eijkel, and A. van den Berg, "Energy conversion in microsystems: Is there a role for micro/nanofluidics?" Lab Chip **7**, 1234 (2007).
[30] B. A. Grimes and A. I. Liapis, "Expressions for evaluating the possibility of slip at the liquid-solid interface in open tube capillary electrochromatography," J. Colloid Interface Sci. **263**, 113 (2003).
[31] L. Bocquet and J. Barrat, "Flow boundary conditions from nano-to micro-scales," Soft Matter **3**, 685 (2007).
[32] J. Eijkel, "Liquid slip in micro- and nanofluidics: Recent research and its possible implications," Lab Chip **7**, 299 (2007).
[33] T. M. Squires, "Electrokinetic flows over inhomogeneously slipping surfaces," Phys. Fluids **20**, 092105 (2008).
[34] D. M. Huang, C. Cottin-Bizonne, C. Ybert, and L. Bocquet, "Massive amplification of surface-induced transport at superhydrophobic surfaces," Phys. Rev. Lett. **101**, 064503 (2008).
[35] A. Ajdari and L. Bocquet, "Giant amplification of interfacially driven transport by hydrodynamic slip: Diffusio-osmosis and beyond," Phys. Rev. Lett. **96**, 186102 (2006).
[36] J. Morthomas and A. Wurger, "Thermophoresis at a charged surface: The role of hydrodynamic slip," J. Phys.: Condens. Matter **21**, 035103 (2009).
[37] A. S. Khair and T. M. Squires, "The influence of hydrodynamic slip on the electrophoertic mobility of a spherical colloidal particle," Phys. Fluids **21**, 042001 (2009).
[38] O. D. Velev and K. H. Bhatt, "On-chip micromanipulation and assembly of colloidal particles by electric fields," Soft Matter **2**, 738 (2006).
[39] A. R. Gingras, N. Bate, B. T. Goult, L. Hazelwood, I. Canestrelli, J. G. Grossmann, H. J. Liu, N. S. M. Putz, G. C. K. Roberts, N. Volkmann, D. Hanein, I. L. Barsukov, and D. R. Critchley, "The structure of the C-terminal actin-binding domain of talin," The European Molecular Biology Organization Journal **27**, 458 (2008).
[40] H. A. Pohl, *Dielectrophoresis* (Cambridge University Press, New York, 1978).
[41] T. B. Jones, *Electromechanics of Particles* (Cambridge University Press, New York, 1995).
[42] H. Liu and H. H. Bau, "The dilelectrophoresis of cylindrical and spherical particles submerged in shells and semi-infinite media," Phys. Fluids **16**, 1217 (2004).
[43] J. Lyklema, *Fundamentals of Interface and Colloid Science. Volume II: Solid-Liquid Interfaces* (Academic, San Diego, 1995).
[44] R. J. Hunter, *Foundations of Colloid Science* (Oxford University Press, New York, 2001).
[45] C. Grosse, S. Pedrosa, and V. N. Shilov, "Corrected results for the influence of size, zeta potential, and state of motion of dispersed particles on the conductivity of a colloidal suspension," J. Colloid Interface Sci. **265**, 197 (2003).
[46] H. Zhou, M. A. Preston, R. D. Tilton, and L. R. White, "Calculation of the electric polarizability of a charged spherical dielectric particle by the theory of colloid electrokinetics," J. Colloid Interface Sci. **285**, 845 (2005).
[47] H. Zhao and H. H. Bau, "The polarization of a non-conducting nano spherical particle in the presence of a thick electric double layer," J. Colloid Interface Sci. **333**, 663 (2009).
[48] C. T. O'Konski, "Electric properties of macromolecules. V. Theory of ionic polarization in polyelectrolytes," J. Phys. Chem. **64**, 605 (1960).
[49] R. W. O'Brien, "The high-frequency dielectric dispersion of a colloid," J. Colloid Interface Sci. **113**, 81 (1986).
[50] D. A. Saville, T. Bellini, V. Degiorgio, and F. Mantegazza, "An extended Maxwell–Wagner theory for the electric birefringence of charged colloids," J. Chem. Phys. **113**, 6974 (2000).
[51] H. Zhao and H. H. Bau, "Effect of double-layer polarization on the forces that act on a nanosized cylindrical particle in an ac electric field," Langmuir **24**, 6050 (2008).
[52] S. S. Dukhin and V. N. Shilov, *Dielectric Phenomena and the Double*

Downloaded 13 Aug 2013 to 131.216.164.149. This article is copyrighted as indicated in the abstract. Reuse of AIP content is subject to the terms at: http://pof.aip.org/about/rights_and_permissions

Layer in Disperse Systems and Polyelectrolytes (Wiley, New York, 1974).
[53]C. Grosse and V. N. Shilov, "Theory of the low-frequency electrorotation of polystyrene particles in electrolyte solution," J. Phys. Chem. **100**, 1771 (1996).
[54]V. N. Shilov and T. S. Simonova, "Polarization of electric double layer of disperse particles and dipolophoresis in a steady (dc) field," Colloid J. USSR **43**, 114 (1981).
[55]R. W. O'Brien, "The response of a colloidal suspension to an alternative electric field," Adv. Colloid Interface Sci. **16**, 281 (1982).
[56]C. S. Mangelsdorf and L. R. White, "Dielectric response of a dilute suspension of spherical colloidal particles to an oscillating electric field," J. Chem. Soc., Faraday Trans. **93**, 3145 (1997).
[57]S. E. Pedrosa and C. Grosse, "Numerical analysis of the concentration polarization in colloid suspension: Comparison with theoretical predictions," J. Colloid Interface Sci. **219**, 37 (1999).
[58]J. J. López-García, J. Horno, A. V. Delgado, and F. Gonzalez-Caballero, "Use of a network simulation method for the determination of the response of a colloid suspension to a constant electric field," J. Phys. Chem. B **103**, 11297 (1999).
[59]J. J. López-García, J. Horno, F. Gonzalez-Caballero, C. Grosse, and A. V. Delgado, "Dynamics of the electric double layer: Analysis in the frequency and time domains," J. Colloid Interface Sci. **228**, 95 (2000).
[60]J. J. López-García, C. Grosse, and J. Horno, "Numerical study of colloid suspensions of soft spherical particles using the network method: 2. AC electrokinetic and dielectric properties," J. Colloid Interface Sci. **265**, 341 (2003).
[61]V. N. Shilov, A. V. Delgado, F. Gonzalez-Caballero, J. Horno, J. J. Lopez-Garcia, and C. Grosse, "Polarization of the electrical double layer: Time evolution after application of an electric field," J. Colloid Interface Sci. **232**, 141 (2000).
[62]C. Chassagne, D. Bedeaux, and G. J. M. Koper, "Dielectric enhancement of charged nanospheres dispersed in an electrolyte," J. Phys. Chem. B **105**, 11743 (2001).
[63]C. Chassagne, D. Bedeaux, and G. J. M. Koper, "Dielectric response of colloidal spheres in non-symmetric electrolytes," Physica A **317**, 321 (2003).
[64]R. J. Hill, D. A. Saville, and W. B. Russel, "High-frequency dielectric relaxation of a spherical colloidal particles," Phys. Chem. Chem. Phys. **5**, 911 (2003).
[65]V. Zimmerman, C. Grosse, and V. N. Shilov, "Numerical calculation of the dynamic dipole coefficient and electrorotation velocity of cells," J. Phys. Chem. B **107**, 14612 (2003).
[66]H. Zhao and H. H. Bau, "The polarization of nanorods submerged in an electrolyte solution and subjected to an ac electric field," Langmuir **26**, 5412 (2010).
[67]K. Zhao and K. He, "Dielectric relaxation of suspensions of nanoscale particles surrounded by a thick electric double layer," Phys. Rev. B **74**, 205319 (2006).
[68]M. Z. Bazant and T. M. Squires, "Induced-charge electro-kinetic phenomena: Theory and microfluidic applications," Phys. Rev. Lett. **92**, 066101 (2004).
[69]T. M. Squires and M. Z. Bazant, "Induced-charge electro-osmosis," J. Fluid Mech. **509**, 217 (2004).
[70]T. M. Squires and M. Z. Bazant, "Breaking symmetries in induced-charge electro-osmosis and electrophoresis," J. Fluid Mech. **560**, 65 (2006).
[71]V. N. Shilov and S. S. Dukhin, "Theory of polarization of diffuse part of a thin double layer at a spherical particle in an alternating electric field," Colloid J. USSR **32**, 90 (1970).
[72]I. N. Simonov and S. S. Dukhin, "Theory of electrophoresis of solid conducting particles in case of ideal polarization of a thin diffuse double-layer," Colloid J. USSR **35**, 173 (1973).
[73]I. N. Simonov and V. N. Shilov, "Theory of the polarization of the diffuse part of a thin double layer at conducting, spherical particles in an alternating electric field," Colloid J. USSR **35**, 350 (1973).
[74]I. N. Simonov and V. N. Shilov, "Theory of low-frequency dielectric-dispersion of a suspension of ideally polarizable spherical-particles," Colloid J. USSR **39**, 775 (1977).
[75]H. Zhao and H. H. Bau, "On the effect of induced electro-osmosis on a cylindrical particle next to a surface," Langmuir **23**, 4053 (2007).
[76]R. W. O'Brien and L. R. White, "Electrophoretic mobility of a spherical colloidal particle," J. Chem. Soc., Faraday Trans. 2 **74**, 1607 (1978).
[77]F. Booth, "Sedimentation potential and velocity of solid spherical particles," J. Chem. Phys. **22**, 1956 (1954).
[78]D. A. Saville, "Electrokinetic effects with small particles," Annu. Rev. Fluid Mech. **9**, 321 (1977).
[79]R. W. O'Brien, "The electric conductivity of a dilute suspension of charged particles," J. Colloid Interface Sci. **81**, 234 (1981).
[80]A. B. Basset, *A Treatise on Hydrodynamics* (Dover, New York, 1961).

Downloaded 13 Aug 2013 to 131.216.164.149. This article is copyrighted as indicated in the abstract. Reuse of AIP content is subject to the terms at: http://pof.aip.org/about/rights_and_permissions